Osteoarthritis and Cartilage 32 (2024) 1552–1565

Osteoarthritis and Cartilage

Disentangling the detrimental effects of local from systemic adipose tissue dysfunction on articular cartilage in the knee

Jessica J. McClure #, George D. McIlroy †, Rebecca A. Symons #, Susan M. Clark #, Iain Cunningham #, Weiping Han ‡, Karolina Kania #, Fabio Colella #, Justin J. Rochford †, Cosimo De Bari #, Anke J. Roelofs # *

Arthritis & Regenerative Medicine Laboratory, Centre for Arthritis and Musculoskeletal Health, University of Aberdeen, Foresterhill, Aberdeen AB25 2ZD, UK
† *The Rowett Institute and Aberdeen Cardiovascular and Diabetes Centre, University of Aberdeen, Foresterhill, Aberdeen AB25 2ZD, UK*
‡ *Institute of Molecular and Cell Biology, Agency for Science, Technology and Research (A*STAR), Singapore*

ARTICLE INFO

Article history:
Received 7 February 2024
Accepted 12 July 2024

Keywords:
Osteoarthritis
Obesity
Infrapatellar fat pad
Articular cartilage
Lipodystrophy

SUMMARY

Objective: Obesity increases osteoarthritis (OA) risk due to adipose tissue dysfunction with associated metabolic syndrome and excess weight. Lipodystrophy syndromes exhibit systemic metabolic and inflammatory abnormalities similar to obesity without biomechanical overloading. Here, we used lipodystrophy mouse models to investigate the effects of systemic versus intra-articular adipose tissue dysfunction on the knee.
Methods: Intra-articular adipose tissue development was studied using reporter mice. Mice with selective lipodystrophy of intra-articular adipose tissue were generated by conditional knockout (cKO) of *Bscl2* in *Gdf5*-lineage cells, and compared with whole-body *Bscl2* knockout (KO) mice with generalised lipodystrophy and associated systemic metabolic dysfunction. OA was induced by surgically destabilising the medial meniscus (DMM) and obesity by high-fat diet (HFD). Gene expression was analysed by quantitative RT-PCR and tissues were analysed histologically.
Results: The infrapatellar fat pad (IFP), in contrast to overlying subcutaneous adipose tissue, developed from a template established from the *Gdf5*-expressing joint interzone during late embryogenesis, and was populated shortly after birth by adipocytes stochastically arising from *Pdgfrα*-expressing *Gdf5*-lineage progenitors. While female *Bscl2* KO mice with generalised lipodystrophy developed spontaneous knee cartilage damage, *Bscl2* cKO mice with intra-articular lipodystrophy did not, despite the presence of synovial hyperplasia and inflammation of the residual IFP. Furthermore, male *Bscl2* cKO mice showed no worse cartilage damage after DMM. However, female *Bscl2* cKO mice showed increased susceptibility to the cartilage-damaging effects of HFD-induced obesity.
Conclusion: Our findings emphasise the prevalent role of systemic metabolic and inflammatory effects in impairing cartilage homeostasis, with a modulatory role for intra-articular adipose tissue.

Introduction

Osteoarthritis (OA) is highly associated with obesity, with cartilage degeneration resulting from a combination of biomechanical, metabolic and inflammatory factors caused by increased adiposity.[1] A hallmark of obesity is generalised adipose tissue dysfunction, characterised by hypertrophic adipose tissue expansion, altered adipokine secretion, and immune cell infiltration, leading to the clinical picture of metabolic syndrome with systemic inflammation.[2] Adipose tissue homeostasis is therefore important for metabolic health, and development and function of adipose tissue depots are being extensively investigated. The adipocytes of white adipose tissue (WAT) originate from precursor cell populations marked by the expression of Pdgfrα,[3] with timing of development dependent on anatomical location. In mice, subcutaneous white adipose tissue (sWAT) develops between embryonic day (E)14–18, while visceral white adipose tissue (vWAT) develops postnatally.[4]

Abnormalities in intra-articular adipose tissue, especially the infrapatellar fat pad (IFP) in the knee, have been linked with

* Correspondence to: Institute of Medical Sciences, University of Aberdeen, Foresterhill, Aberdeen AB25 2ZD, UK.
E-mail address: a.roelofs@abdn.ac.uk (A.J. Roelofs).

https://doi.org/10.1016/j.joca.2024.07.006

cartilage damage in OA. The IFP is dysfunctional in knee OA, with high levels of pro-inflammatory adipokines and cytokines such as tumour necrosis factor alpha (TNFα).[5] The anatomical proximity of intra-articular adipose depots may potentiate these inflammatory and catabolic mediators acting on joint tissues. Adipokines can stimulate the production of inflammatory mediators and matrix metalloproteinases (MMPs), which promote cartilage catabolism.[6] In addition, increased immune cell infiltration in the IFP of OA patients can further contribute to the secretion of inflammatory factors.[7] Therefore, the ability of the IFP to generate a proinflammatory and catabolic environment indicates that this adipose depot could impair cartilage health in OA.

Adipose tissue dysfunction is also present in congenital generalised lipodystrophies (CGL).[8] CGL are a group of disorders in which significantly impaired adipose tissue formation and maintenance throughout the body is accompanied by systemic inflammation and severe metabolic dysfunction. There are similarities to the metabolic syndrome associated with obesity but without the biomechanical joint overload of excessive adiposity.[9,10] Lipodystrophic mice additionally display inflammatory features within the residual adipose tissue.[11,12] CGL type 2 (CGL2), caused by mutations in the gene *BSCL2* which encodes the protein Seipin,[13] is a severe form of lipodystrophy characterised by an almost complete lack of adipose tissue and severe metabolic complications including hepatic steatosis and insulin resistance. Seipin is an endoplasmic reticulum membrane protein involved in adipogenesis and lipid droplet formation.[14,15] CGL2 has been modelled using *Bscl2* knockout (KO) mice, which recapitulate the metabolic phenotype and pattern of adipose tissue loss observed in CGL2 patients.[10,16] Unlike some other CGL subtypes, CGL2 displays marked reduction in intra-articular adipose tissue volume in depots such as the IFP.[17,18]

Here, we employed lipodystrophy mouse models to disentangle the effects of local from systemic adipose tissue dysfunction on joint health. Female mice with lipodystrophy restricted to intra-articular adipose tissue through conditional KO of *Bscl2* in the developing joints showed inflammation of the residual IFP, similar to mice with CGL. In contrast, they did not develop spontaneous cartilage damage with age, nor did they show altered cartilage damage following surgical induction of OA using the DMM model. However, they showed exacerbated cartilage damage after high-fat diet (HFD)-induced obesity. Our findings indicate that systemic adipose tissue dysfunction is a main driver for loss of articular cartilage homeostasis and can synergise with intra-articular adipose tissue dysfunction in mediating joint degeneration.

Materials and methods

Mice

All animal experimental protocols were approved by the UK Home Office and the University of Aberdeen Animal Welfare and Ethical Review Committee. Experiments were designed to ensure that minimum numbers of mice were used to obtain biologically significant results. All animal experiments were performed at the University of Aberdeen Medical Research Facility after an acclimatisation period of at least 6 days. Mice were group-housed with up to 10 mice per cage in the same room under standard conditions, at 20–22 °C on a 12 h/12 h light/dark cycle, with ad libitum access to water and standard chow (CRM (P) 801722, Special Diets Services), or an HFD containing 60% kcal from fat (D12492, Research Diets) for 14–15 weeks. IFP development was studied using *Gdf5-Cre,*[19] Cre-inducible *tdTomato* (*Tom*),[20] Cre-inducible *Confetti*,[21] and *Pdgfrα-H2BGFP*[22] reporter mouse lines (see Suppl. Table 1). *Bscl2*$^{fl/fl}$ and *Bscl2* KO mice were previously generated[10,23] (see Suppl. Table 1). *Gdf5-Cre* mice were on an FVB background while other mouse lines were on a C57Bl/6 background. Mice with conditional ablation of *Bscl2* in developing joints were generated by crossing *Gdf5-Cre* mice with *Bscl2*$^{fl/fl}$ mice to generate *Gdf5-Cre*;*Bscl2*$^{fl/fl}$ (*Bscl2* cKO) mice. To confirm targeting of intra-articular adipose tissue, a Cre-inducible *Tom* reporter allele[20] was crossed in. Genotyping was performed by PCR using DNA extracted from earclips and post-mortem tissue biopsies. Genotype, sex and age of *Bscl2* KO and *Bscl2* cKO mice and their littermate genotype controls included in the study are indicated in Suppl. Tables 2 and 3, respectively. No formal randomisation protocol was used as group allocation was based on genotypes. However, for each experiment, the average age of the two groups (control and KO/cKO) was matched within 1 week of each other. Mice with leaky Tom expression, detected as previously described,[24] were excluded a priori or at the analysis stage. Other exclusions are indicated in Suppl. Table 3. The fat mass of mice was measured immediately post-mortem using an EchoMRI™−500 body composition analyser (Zinsser Analytic GmbH), and measurements were normalised to body weight as described.[10]

Metabolic studies

Glucose tolerance test (GTT) and insulin tolerance test (ITT) were performed after 10 and 11 weeks of HFD-feeding, respectively, as previously described.[10] Briefly, basal glucose readings (0 min) were taken from mice fasted for 5 h by glucometer readings (AlphaTrak® II, Zoetisus) from tail punctures. For GTT, mice were given a 2 mg/g D-glucose (Sigma) bolus by intraperitoneal injection, and blood glucose levels were monitored after 15, 30, 60, and 120 min. For ITT, mice were given a 0.75 mU/g insulin bolus by intraperitoneal injection, and blood glucose levels were monitored at 15, 30, 60, 90, and 120 min following injection. Metabolic experiments were performed at a consistent time of day.

Destabilisation of the medial meniscus

Surgery was performed to induce destabilisation of the medial meniscus (DMM) in 3-month-old male *Bscl2* cKO and genotype control mice (Suppl. Table 3) via resection of the medial meniscotibial ligament in the left knee as a model of post-traumatic OA.[25] Male mice were used in these experiments since female mice are known to be resistant to cartilage damage in response to DMM.[26] Mice were anaesthetised by intraperitoneal injection of ketamine (50 mg/kg) and medetomidine (0.67 mg/kg) with subcutaneous atipamezole (1 mg/kg) post-operatively or through inhalation of isoflurane with subcutaneous buprenorphine (0.1 mg/kg) peri- and post-operatively. The contralateral (right) knee remained unoperated and served as internal control. Mice were humanely killed at 6 weeks post-surgery and hindlimbs were dissected for histological analysis. Data were collected from 3 separate experiments, with similar numbers of genotype control and *Bscl2* cKO mice in each experiment. For 2 experiments, the order of surgery was random, whereas in 1 experiment, the genotype control mice were operated first.

Micro-CT analysis

After mice were humanely killed, hindlimbs were dissected and fixed in 4% paraformaldehyde overnight, then scanned at 40x magnification using a Skyscan 1072 micro-computed tomography (micro-CT) system (Bruker) as previously described,[27] with an isotropic voxel size of 7.32 μm. Images were reconstructed using NRecon 2.0.4.0 and visualised using DataViewer 1.5.6.2 and CTvox 3.3 (Bruker). Analysis of subchondral bone was carried out using CTAn v1.13 as described.[27]

Histological analysis

After mice were humanely killed, hindlimbs were dissected, fixed in 4% paraformaldehyde, decalcified in 10% ethylenediaminetetraacetic acid (EDTA), and paraffin-sectioned at 5 μm thickness or cryo-sectioned at 10 μm thickness in a sagittal orientation starting from the medial side. Adipose tissue depots, including the infrapatellar, inguinal, and perigonadal WAT, and interscapular brown adipose tissue (BAT), were dissected and immediately snap-frozen and stored at −70 °C. Inguinal and perigonadal WAT samples were later defrosted, fixed in 4% paraformaldehyde, and paraffin-sectioned at 5 μm thickness. Tissue sections were stained with safranin O and fast green, haematoxylin and eosin (H&E), alcian blue and nuclear fast red, or picrosirius red, according to standard protocols. Immunohistochemistry (IHC) and immunofluorescence stainings were performed as previously described,[28] using antibodies listed in Suppl. Table 4. Images were acquired on a Zeiss Axioscan Z1, Zeiss Axioscope 5 or Zeiss Axioskop 40 microscope, or Zeiss LSM710 confocal microscope, with ZEN software.

IFP image analysis

The IFP was analysed at its largest sagittal cross-sectional area defined by anatomical landmarks within the joint, namely where the posterior cruciate ligament is widest and at the point where the anterior and posterior cruciate ligaments cross. Adipocytes were quantified from slide-scanned images of H&E-stained tissue sections within the entire IFP cross-sectional area via a semi-automated method using QuPath v0.1.2[29] and ImageJ. First, background and noise were removed, and red/green/blue images were converted to binary images. A Gaussian blur was applied and segmentation performed using a watershed algorithm.[30] A threshold was applied consistently across all images. The "analyse particles" command established ROIs and inaccurately detected adipocyte ROIs were deleted or manually edited. Blood vessels and IFP size were measured using the brush or polygon tool. The number of macrophages within the entire IFP cross-sectional area was manually counted from slide-scanned images of sections stained immunohistochemically for CD68 using QuPath v0.2.3, and macrophage counts were normalised to IFP size. In mice with Tom expression, the percentage of Tom+ adipocytes was quantified from confocal microscopy images of sections co-stained for perilipin by immunofluorescence, using Zen 3.4 or QuPath v0.1.2 software. All quantification was performed by researchers blinded to experimental groups, and data are presented as averaged values from 2–3 sections per sample.

Histopathological image analysis

Articular cartilage histopathology was assessed as primary outcome measure, from sections stained with safranin O and fast green according to the OsteoArthritis Research Society International (OARSI) histopathology criteria.[31] Sections were selected (8–17 per sample) at set intervals across the medial compartment of the knee. Images were analysed independently by at least 2 researchers blinded to experimental groups and data averaged between scorers for each sample. The tibial and femoral scores were summed for each section to yield a maximum score of 12, with data presented as the average of the highest 5 scores for each sample to account for variable lesion severity across the articular cartilage surface. Synovial cellularity was assessed from sections stained with H&E that were also used for adipocyte histomorphometric analysis, on a scale from 0 (normal) to 3 (strongly hyperplastic) according to previously published scoring criteria.[32] Images were analysed independently by 2 researchers blinded to experimental groups and data were averaged for each sample.

Gene expression analysis

After mice were humanely killed, adipose tissue depots, including the infrapatellar, inguinal, and perigonadal WAT, and interscapular BAT, were dissected and immediately snap-frozen and stored at −70 °C. RNA was extracted using TRIZOL reagent according to standard protocols or using the RNeasy mini kit (Qiagen) and quantitative reverse transcription polymerase chain reaction (RT-qPCR) was performed as previously described.[10,27] Primers were designed using Primer-BLAST (NCBI) or TaqMan assays were used (Thermofisher), listed in Suppl. Tables 5 and 6. Primers were validated by melting curve analysis and/or gel electrophoresis. Data were analysed using a standard-curve method and normalised to the expression of reference genes (*Nono, Hprt* and/or *Ywhaz*). Amplification efficiencies of all primer pairs were between 1.8 and 2.0.

Statistical analysis

All data points on graphs and n-numbers in text indicate individual mice. Lines and error bars on graphs indicate mean ± 95% confidence interval (CI). Statistical tests were performed using GraphPad Prism v5 or SigmaPlot v14. The tests used to determine statistical significance ($p < 0.05$) are indicated in figure legends. Shapiro-Wilk and Brown-Forsythe tests were performed to assess normality and equal variance, respectively. Log transformation was used to equalise variance prior to statistical testing where indicated. Ordinal data were analysed using a non-parametric Mann-Whitney U test. A Grubb's test, at significance level $p < 0.01$, was performed using the online GraphPad outlier calculator to statistically identify an outlier in the OARSI score data from the genotype control group of the mice fed an HFD, with a score of 4.45. This mouse was excluded from all presented data.

Results

Female mice with generalised lipodystrophy spontaneously develop cartilage damage

To investigate the effect on the knee of generalised lipodystrophy, we analysed *Bscl2* KO mice, which recapitulate the effects of CGL2 observed in humans, characterised by very low adipose tissue mass and severe metabolic dysfunction.[10,16] Since females are reported to be clinically more severely affected than males,[33,34] we analysed female and male mice separately. Histological analysis of knees from *Bscl2* KO mice showed the presence of a fibrous IFP-like tissue that was decreased in size ($p < 0.0001$) with a greatly decreased adipocyte number ($p < 0.0001$) in both female and male *Bscl2* KO mice compared to genotype controls (Fig. 1A–C; Suppl. Figure 1A). The residual adipocytes in female *Bscl2* KO mice were on average larger than the adipocytes in the genotype controls ($p = 0.02$; Fig. 1B), indicative of hypertrophy. Interestingly, this was not observed in male mice (Fig. 1C). Compared to controls, the IFP of *Bscl2* KO mice showed an increase in CD68+ macrophages ($p < 0.0001$; Fig. 1D; Suppl. Figure 1B) and elevated expression of the pro-inflammatory cytokine *Tnfα* ($p = 0.03$; Fig. 1E; Suppl. Figure 1C), in keeping with the increased macrophage infiltration and inflammation reported in residual white adipose tissue in lipodystrophic mouse models.[11,12] In addition, a significant increase in blood vessel number ($p < 0.0001$) and mean size ($p = 0.003$; Fig. 1F; Suppl. Figure 1D), as well as infiltration of mast cells detected by alcian blue staining (Suppl. Figure 1E), were observed within the IFP of *Bscl2* KO mice. Furthermore, picrosirius red staining revealed extensive fibrosis of the IFP (Suppl. Figure 1F), and the synovium surrounding the IFP was hyperplastic in the *Bscl2* KO mice compared to genotype controls ($p < 0.001$; Fig. 1G; Suppl. Figure 1G). Analysis of the articular cartilage of the knee revealed modest but significantly increased

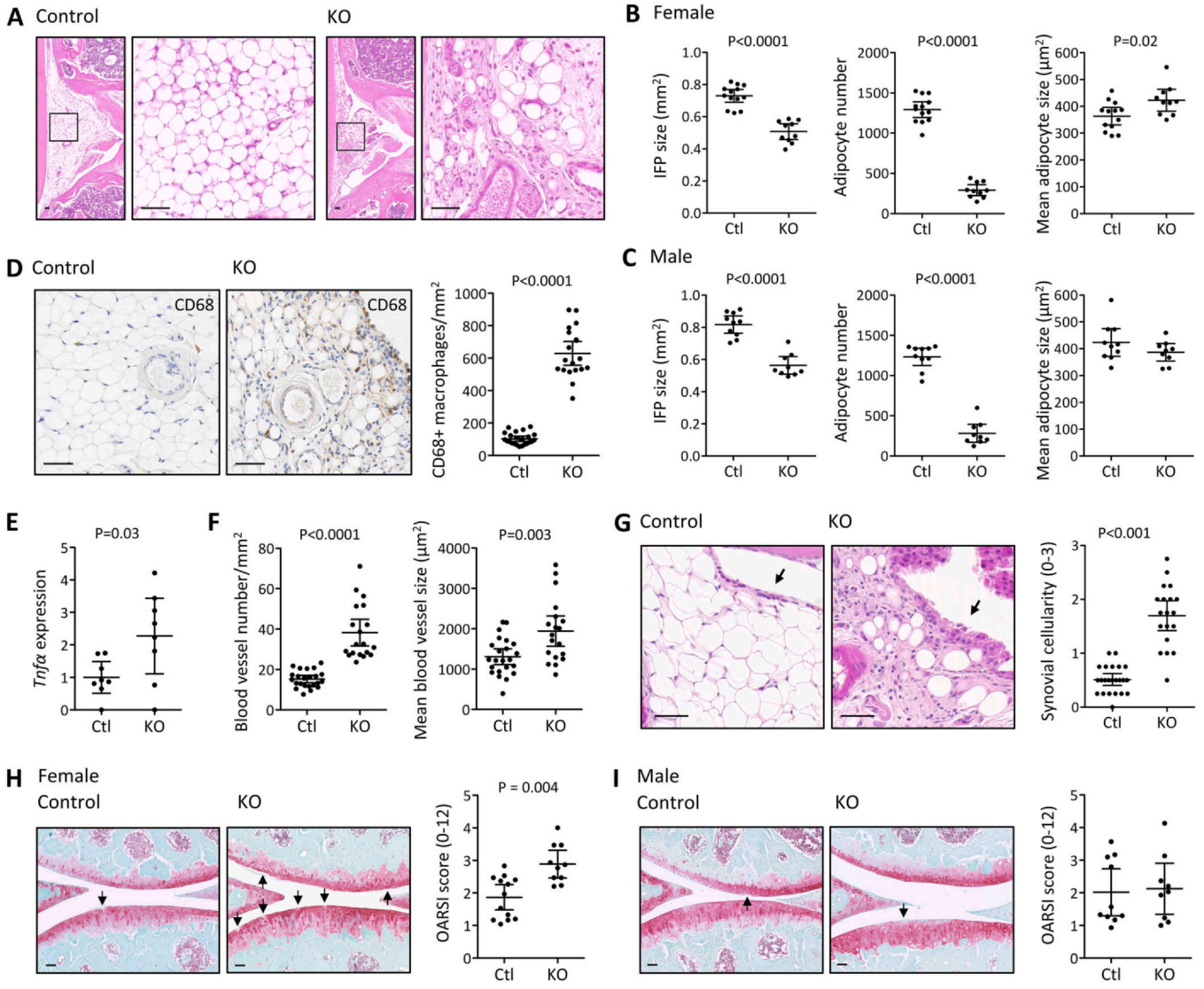

Fig. 1

Osteoarthritis and Cartilage

Effect of generalised lipodystrophy on the adult knee. Shown are pooled data from 5 cohorts of *Bscl2* KO and genotype control (Ctl) mice analysed at 4–6 months of age. (**A**) Typical morphology of the IFP, visualised by H&E staining. (**B,C**) IFP size, adipocyte number, and mean adipocyte size of 13 control and 10 *Bscl2* KO females (**B**), and 10 control and 9 *Bscl2* KO males (**C**), quantified from H&E-stained sections. P-values: unpaired two-tailed Student's t-test. (**D**) Macrophages within the IFP of 23 control and 19 *Bscl2* KO mice, detected by CD68 IHC (brown) with haematoxylin counterstain (blue). P-value: unpaired two-tailed Student's t-test after log transformation. (**E**) Expression of *Tnfa* in the IFP of 8 control and 8 *Bscl2* KO mice, quantified by RT-qPCR and shown relative to the average in the control group. P-value: unpaired two-tailed Student's t-test. (**F**) Blood vessel number and size within the IFP of 23 control and 19 *Bscl2* KO mice, quantified from H&E-stained sections. P-values: unpaired two-tailed Student's t-test after log transformation. (**G**) Cellularity of the synovium surrounding the IFP (arrows) in 23 control and 19 *Bscl2* KO mice, scored from H&E-stained sections. P-value: Mann-Whitney U test. (**H,I**) Articular cartilage damage in 13 control and 10 *Bscl2* KO females (**H**), and 10 control and 9 *Bscl2* KO males (**I**), quantified from safranin O and fast green-stained sections. Arrows indicate cartilage lesions. OARSI scores are shown as the average of the highest 5 summed tibia and femur scores. P-values: Mann-Whitney U test. Lines and error bars on all graphs indicate mean ± 95% CI. All images shown are from female mice, unless otherwise indicated, and scale bars indicate 50 µm. See Suppl. Figure 1A for H&E images of the IFP from male mice, and Suppl. Figure 1B-D,G for data in (**D-G**) separated by females and males.

damage in female *Bscl2* KO mice compared to genotype controls at around 5 months of age (p = 0.004; Fig. 1H), while there was no difference in males (Fig. 1I). Together, these findings reveal that mice with CGL and associated systemic metabolic dysfunction show inflammatory features within the residual IFP, which in females is associated with cartilage damage in the knee.

Intra-articular adipocytes arise from Gdf5-expressing progenitor cells in early postnatal life

To understand whether the cartilage damage in female *Bscl2* KO mice is driven by local or systemic adipose tissue dysfunction, we studied the process of IFP development in order to devise a way to

induce selective lipodystrophy in the knee. Previous lineage tracing studies revealed that *Gdf5*-expressing progenitor cells within the embryonic joint interzones give rise to the joint tissues, including articular cartilage, ligaments, and parts of the synovium during development.[19,35] To gain insight into IFP formation, we performed a systematic analysis from embryonic joint development into early postnatal life. Analysis of *Gdf5-Cre;tdTom* embryos from E14.5 onwards showed that the presumptive IFP develops as a fibrous-like template derived from *Gdf5*-expressing joint interzone progenitors (Fig. 2A). The first small adipocytes, detected by staining for the adipocyte marker perilipin, appeared at postnatal day (P)1, followed by a gradual increase in the number and size of adipocytes until the IFP was established at P6 (Fig. 2B). Analysis of Tom expression, indicating joint interzone derivation, and a green fluorescent protein (GFP) reporter controlled by the *Pdgfrα* promoter to identify adipocyte precursor cells,[3] showed newly forming adipocytes developing from Tom+GFP+ progenitors at P2 (Fig. 2C). At P5, more mature adipocytes were interspersed throughout the IFP, with Tom+GFP+ progenitors enriched around blood vessels (Fig. 2C). Virtually all adipocytes and GFP+ progenitors in the IFP expressed Tom (Fig. 2C), indicative of *Gdf5*-lineage derivation.

In adult mice at 3 months of age, virtually all adipocytes in the IFP were still positive for Tom, as were the interspersed GFP+ cells (Suppl. Figure 2A), indicating persistence through adulthood. Similarly, intra-articular adipose tissue in ankle and elbow joints showed an abundance of Tom+ cells (Suppl. Figure 2A), while intra-articular adipose tissue in more proximal shoulder and hip joints showed partial labelling of adipocytes and GFP+ cells with Tom (Suppl. Figure 2B). Clonal lineage mapping using *Gdf5-Cre;Confetti* mice revealed small clonal adipocyte clusters interspersed throughout the IFP (Fig. 2D), indicating that adipocytes form within local niches from resident progenitors. IFP adipocytes remained of *Gdf5*-lineage ontogeny up to at least 12 months of age (Fig. 2E). In contrast, the overlying sWAT was already established at birth (Fig. 2B) and of distinct ontogeny (Fig. 2E).

Together, these data spatiotemporally define IFP formation and establish that intra-articular adipocytes in the knee and other distal synovial joints have a unique ontogenic derivation from the embryonic joint interzone that persists through adult life and can be selectively targeted using *Gdf5-Cre* mice.

Mice with intra-articular lipodystrophy do not develop cartilage damage

To decipher the influence of the IFP on joint homeostasis, we induced lipodystrophy in the knee by crossing *Gdf5-Cre* mice with *Bscl2*$^{fl/fl}$ mice to generate *Bscl2* cKO mice. As expected, there was no difference in whole-body percent fat mass, as determined by EchoMRI, between the *Bscl2* cKO mice and their genotype controls (Fig. 3A). *Bscl2* cKO mice showed an approximately 5-fold decrease in *Bscl2* expression within the IFP ($p < 0.001$), concomitant with similar decreases in expression of the adipocyte-lineage marker genes *Pparγ* and *Fabp4*, while expression of these genes in sWAT (inguinal), vWAT (perigonadal), and BAT (interscapular) was not significantly different from genotype controls (Fig. 3B). These findings confirm selective targeting of the intra-articular adipose tissue.

Both female and male *Bscl2* cKO mice developed a markedly smaller IFP ($p \leq 0.001$) with a significantly lower adipocyte number ($p < 0.0001$), but no difference in average adipocyte size, when compared to genotype control mice (Fig. 3C–E; Suppl. Figure 3A). This was associated with decreased expression of adipokines in the IFP of *Bscl2* cKO mice compared to controls, as expected (Suppl. Figure 3B). As observed in the congenital *Bscl2* KO model (Fig. 1A–C), residual adipocytes were present in the IFP. To investigate their ontogeny, the Cre-inducible Tom reporter was crossed into the *Bscl2* cKO model. This showed highly efficient targeting of residual adipocytes (99.4% Tom+, 95% CI [99.0%, 99.9%]) (Fig. 3F), confirming their derivation from the *Gdf5*-lineage and excluding compensation from other lineages.

Histological analysis displayed an increased number of CD68+ macrophages within the lipodystrophic IFP of both female and male *Bscl2* cKO mice compared to controls ($p < 0.0001$; Fig. 3G; Suppl. Fig. 3C), as well as increased expression of *Tnfα* ($p = 0.04$, Fig. 3H, Suppl. Figure 3D). In addition, *Bscl2* cKO mice showed an increased number ($p < 0.0001$) and mean size of blood vessels ($p = 0.03$) (Fig. 3I; Suppl. Figure 3E) and mast cell infiltration (Suppl. Figure 3F) within the IFP compared to genotype controls. Increased fibrosis (Suppl. Figure 3G) and hyperplasia of the synovium surrounding the IFP ($p < 0.001$; Fig. 3J,K; Suppl. Figure 3H) were also evident. In contrast, extra-articular WAT depots in cKO mice showed normal tissue morphology (Suppl. Figure 4A), with no overt differences compared to genotype control mice in the presence of macrophages (Suppl. Figure 4B), mast cells (Suppl. Figure 4C), or fibrosis (Suppl. Figure 4D). Expression levels of adipokines and inflammatory cytokines were also similar to genotype control mice (Suppl. Figure 4E), confirming preservation of systemic adipose tissue function in cKO mice. Together, these data show inflammation in the IFP of *Bscl2* cKO mice, which is restricted to the intra-articular adipose tissue in this model. Despite these profound changes to the IFP, the articular cartilage in 3-month-old *Bscl2* cKO mice was not overtly different from that of genotype control mice (Fig. 3K).

Decreased IFP adiposity persisted in female mice at 12 months of age, and hypertrophy of residual adipocytes became apparent ($p < 0.001$; Fig. 4A,B). The presence of inflammatory features that were observed in younger *Bscl2* cKO mice, including macrophage infiltration (Fig. 4C), mast cell infiltration (Suppl. Figure 5A), increased vascularity (Fig. 4D), fibrosis (Suppl. Figure 5B) and synovial hyperplasia (Fig. 4E), also remained evident. Nevertheless, analysis of articular cartilage (Fig. 4F) and tibial subchondral bone (Fig. 4G,H) showed no difference between genotype control and *Bscl2* cKO mice, indicating that intra-articular lipodystrophy did not affect knee joint maintenance throughout adulthood.

To ascertain whether intra-articular lipodystrophy affects OA development in response to joint trauma, the DMM model was used. Six weeks after OA induction, the cartilage of DMM knees showed significant damage compared to contralateral control knees in both control ($p < 0.001$) and *Bscl2* cKO mice ($p = 0.005$), with no difference in the severity of DMM-induced cartilage damage between the two groups of mice (Fig. 4I).

Together, these data indicate that intra-articular lipodystrophy does not significantly affect joint development or maintenance up to at least 12 months of age or OA development in a post-traumatic OA model, despite abnormalities and inflammatory features within the residual IFP similar to those observed in generalised lipodystrophy.

Intra-articular lipodystrophy exacerbates cartilage damage in mice with HFD-induced obesity

To study the effect of obesity in mice with intra-articular lipodystrophy, we administered a HFD to female mice from 2 months of age for a duration of 14–15 weeks. A significant increase in body weight confirmed induction of obesity, with similar weight gain between *Bscl2* cKO and genotype controls over the course of HFD feeding (Fig. 5A). Additionally, there was no obvious difference in systemic metabolic function between the two groups (Fig. 5B,C).

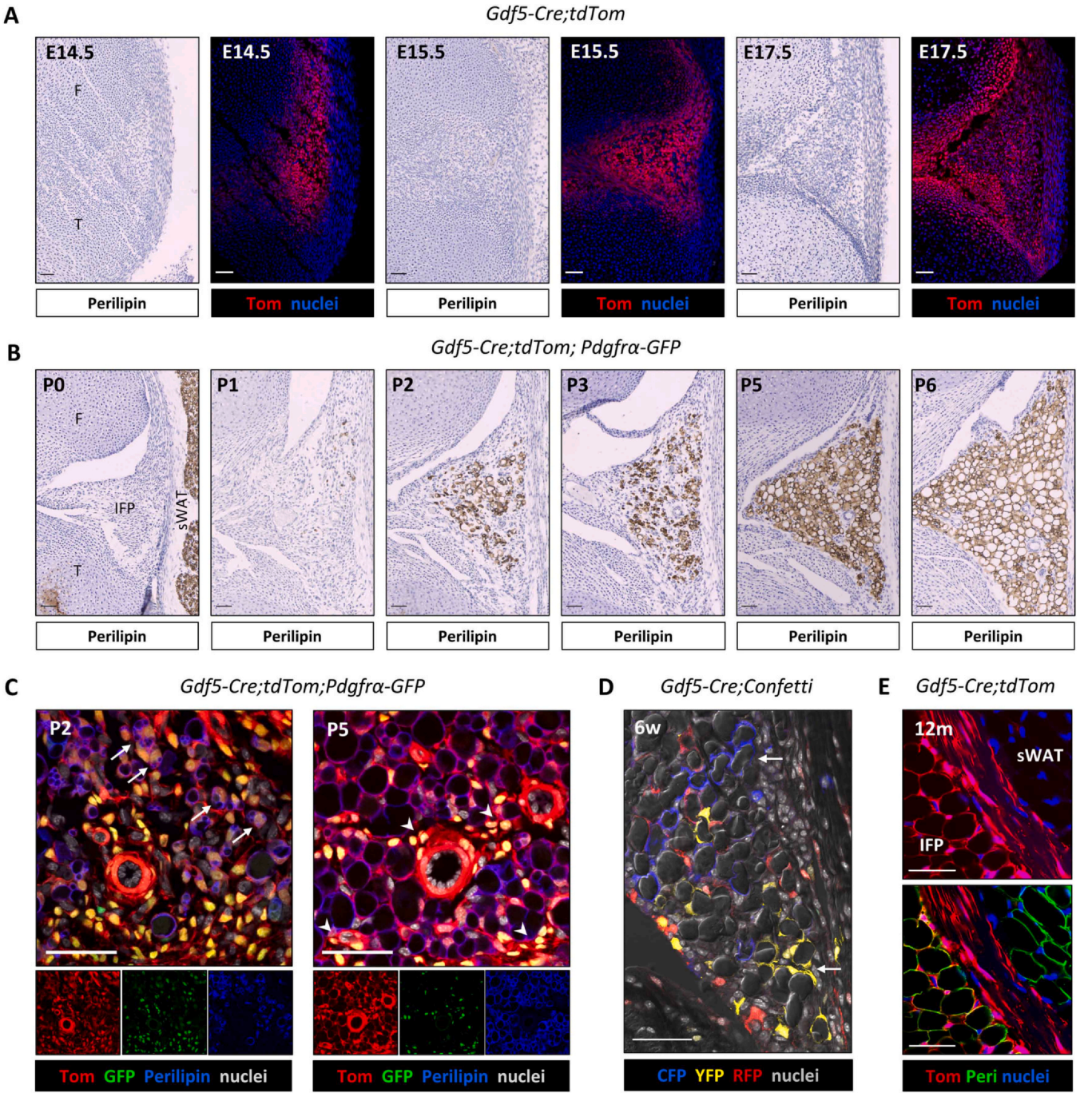

(caption on next page)

Fig. 2 Osteoarthritis and Cartilage

IFP development from *Gdf5*-lineage progenitors. (**A**) Representative microscopy images of *Gdf5-Cre;tdTom* embryos at E14.5 to E17.5 (n = 4–6 per timepoint), showing formation of the IFP template from Tom-expressing cells (red, with DAPI nuclear counterstain in blue) in the developing knee, prior to the appearance of adipocytes as indicated by lack of detectable perilipin by IHC. (**B**) Representative microscopy images of perilipin detected by IHC (brown) with haematoxylin counterstain (blue) in the developing IFP of *Gdf5-Cre;tdTom;Pdgfrα-H2BGFP* neonates from postnatal day (P)0 to P6 (n = 3–4 per time point). (**C**) Representative confocal microscopy images of the IFP in *Gdf5-Cre;tdTom;Pdgfrα-H2BGFP* neonates at P2 and P5 (n = 3 per timepoint) showing formation of Tom+ (red) adipocytes from GFP+Tom+ (yellow) progenitors at P2 (arrows), and clusters of perivascular GFP+Tom+ cells at P5 (arrowheads). Perilipin immunostaining is shown in blue and DAPI nuclear counterstain in light grey. Single-channel images are shown below. (**D**) Representative confocal microscopy image of the IFP from *Gdf5-Cre;Confetti* mice (n = 3) showing clonal adipocyte clusters (arrows), traced from *Gdf5*-expressing cells of the embryonic joint interzone, marked by cyan fluorescent protein (CFP; blue), yellow fluorescent protein (YFP; yellow), or red fluorescent protein (RFP; red). Fluorescence image is shown with phase-contrast overlay to visualise adipocytes, with TO-PRO-3 nuclear counterstain shown in light grey. (**E**) Representative confocal microscopy image of the IFP in 12-month-old *Gdf5-Cre;tdTom* mice (n = 3), showing Tom expression (red) by adipocytes in the IFP, contrasted with the absence of Tom+ adipocytes in adjacent sWAT. The same image is shown without (top) or with perilipin (peri) immunostaining (green; bottom), with DAPI nuclear counterstain in blue. Scale bars on all images indicate 50 μm. F, femur; T, tibia; IFP, infrapatellar fat pad; sWAT, subcutaneous white adipose tissue.

Analysis of the IFP revealed similarities to those of chow-fed mice previously analysed (Fig. 3). Adipocyte number and IFP size remained decreased (Fig. 5D,E), as did the expression of adipokines (Fig. 5F), while the number of CD68+ macrophages (Fig. 5G), *Tnfα* expression (Fig. 5H), and synovial cellularity (Fig. 5I) remained increased in mice with intra-articular lipodystrophy compared to genotype controls, indicating that the decreased IFP adiposity and associated inflammation were sustained in *Bscl2* cKO mice following HFD-feeding. In addition, mean adipocyte size was increased ($p = 0.02$; Fig. 5E), indicating adipocyte hypertrophy in mice with intra-articular lipodystrophy compared to genotype controls, similar to what was observed in 12-month-old chow-fed mice (Fig. 4B). However, in contrast to chow-fed mice, analysis of articular cartilage revealed increased cartilage damage in response to HFD-induced obesity in mice with intra-articular lipodystrophy compared to similarly obese genotype controls ($p = 0.009$, Fig. 5J). Overall, these data show that intra-articular adipose tissue dysfunction exacerbates the detrimental effects of HFD-induced obesity on cartilage.

Discussion

Intra-articular adipose tissue dysfunction within the knee has been implicated in OA pathogenesis,[5–7] but whether this is uncoupled from the systemic metabolic and inflammatory effects of obesity, known to affect cartilage,[36] is unclear. Mice with severe CGL due to loss of *Bscl2* exhibit systemic metabolic and inflammatory abnormalities similar to obesity, but without excess weight causing biomechanical joint overloading.[10,16] Here, we report that the articular cartilage in the knee is affected in female, but not male, *Bscl2* KO mice by around 5 months of age, leading us to examine the involvement of the intra-articular adipose dysfunction independent from the systemic metabolic and inflammatory abnormalities. This revealed that the cartilage in mice with selective intra-articular lipodystrophy and otherwise normal major adipose depots was unaffected even at 12 months of age, and showed a degree of DMM-induced cartilage damage similar to the genotype controls. However, their cartilage was more susceptible to the detrimental effects of HFD-induced obesity, despite decreased expression in the IFP of adipokines, previously suggested to exert degenerative effects on articular cartilage.[37,38] These findings emphasise the prevalent role of systemic metabolic and inflammatory effects in impairing cartilage homeostasis and predisposing to OA development, with a modulatory role for intra-articular adipose tissue in the response to systemic drivers of cartilage damage. Together, our study provides support to the emerging notion that weight loss might be disease-modifying for knee OA in patients with comorbid obesity.[39]

Residual white adipose tissue in mouse models of lipodystrophy has been reported to show increased macrophage infiltration and *Tnfα* expression.[11,12] This was also observed in the residual IFP in our study, together with increased vascularity, likely due to pro-angiogenic macrophage activity,[40,41] altogether indicative of an inflammatory tissue microenvironment. Notably, mice with lipodystrophy restricted to the intra-articular adipose tissue showed similar changes, suggesting this is largely driven by local adipose dysfunction rather than systemic disturbances. It is not clear what is causing the adipose tissue inflammation, but this may be multifactorial and could involve pro-inflammatory effects of dysfunctional pre-adipocytes or adipocytes, as well as local lipid dysregulation affecting tissue-resident macrophages.[42] Adipocyte hypertrophy was observed in the IFP of female but not male mice with generalised lipodystrophy. Hypertrophic adipocytes are associated with increased inflammation and secretion of free fatty acids,[43] which may exert detrimental effects on articular cartilage.[44] However, mice with intra-articular lipodystrophy aged to 12 months similarly showed IFP adipocyte hypertrophy, in the absence of cartilage damage. Together, these findings indicate that the adipocyte hypertrophy and inflammation observed within the residual IFP in these models are insufficient to affect cartilage homeostasis. Instead, the cartilage damage in female mice with generalised lipodystrophy may be secondary to a more severe systemic phenotype. It is known that in both partial and generalised lipodystrophies, females have more severe metabolic dysfunction than males,[33,34] although these sex differences may not be as clear in mice.[45]

Recently, it was reported that mice with generalised lipodystrophy resulting from diphtheria toxin A (DTA)-mediated ablation of adiponectin-expressing cells showed reduced spontaneous OA compared to control mice.[46] Though primarily a marker of adipocytes, adiponectin is also expressed by other cell types, including myocytes and osteoblasts,[47] which may also have been at least partly ablated in this model. In addition, DTA-mediated cell ablation models can be susceptible to off-target effects.[48] These factors may have confounded the observed effects. We cannot exclude the possibility of confounding effects due to loss of Seipin in non-adipocyte-lineage cells in our models, particularly the synovial lining or

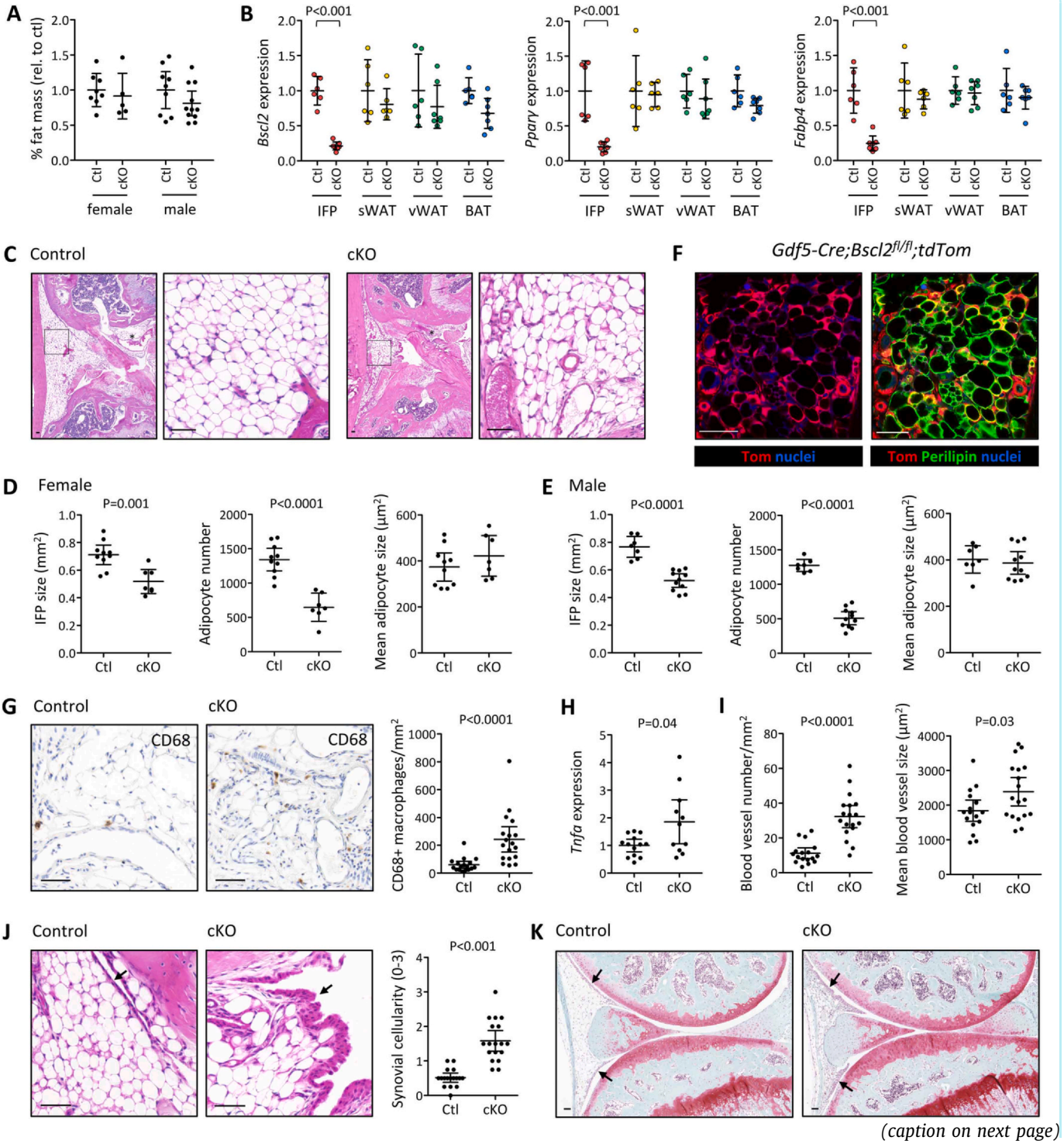

(caption on next page)

Fig. 3 Osteoarthritis and Cartilage

Effect of intra-articular lipodystrophy on the knee. Shown are pooled data from 2 cohorts of *Bscl2* cKO and genotype control (Ctl) mice analysed at 3–4 months of age. (**A**) Percent fat mass of 8 control and 5 *Bscl2* cKO females and 9 control and 11 *Bscl2* cKO males. Data are shown relative to the average of the genotype control group within each cohort. (**B**) Expression of *Bscl2*, *Pparγ*, and *Fabp4* in adipose depots from 6 control (4 females and 2 males) and 7 *Bscl2* cKO mice (3 females and 4 males). Data from sWAT of one *Bscl2* cKO mouse is missing due to low RNA yield. IFP, infrapatellar fat pad; BAT, brown adipose tissue; sWAT, subcutaneous adipose tissue; vWAT, visceral adipose tissue. P-values: two-way ANOVA with Tukey's post-test. (**C**) Typical morphology of the IFP, visualised by H&E staining. Note also lipodystrophy of posterior intra-articular adipose tissue (asterisks) in *Bscl2* cKO mice. (**D,E**) IFP size, adipocyte number, and mean adipocyte size in 10 control and 7 *Bscl2* cKO females (**D**), and 7 control and 11 *Bscl2* cKO males (**E**), quantified from H&E-stained sections. P-values: unpaired two-tailed Student's t-test. (**F**) Tom+ adipocytes (red) within the IFP of a *Bscl2* cKO mouse additionally carrying a Cre-inducible Tom reporter (image representative of 6 mice). The same image is shown with or without perilipin immunostaining (green), with DAPI nuclear counterstain (blue). (**G**) Macrophages within the IFP of 17 control and 18 *Bscl2* cKO mice, detected by CD68 IHC (brown) with haematoxylin counterstain (blue). P-value: unpaired two-tailed Student's t-test after log transformation. (**H**) Expression of *Tnfa* in the IFP of 13 control and 11 *Bscl2* KO mice, quantified by RT-qPCR and shown relative to the average in the control group. P-value: unpaired two-tailed Student's t-test after log transformation. (**I**) Blood vessel number and size within the IFP of 17 control and 18 *Bscl2* cKO mice, quantified from H&E-stained sections. P-values: unpaired two-tailed Student's t-test after and without log transformation, respectively. (**J**) Cellularity of the synovium surrounding the IFP (arrows) in 17 control and 18 *Bscl2* cKO mice, scored from H&E-stained sections. P-value: Mann-Whitney U test. (**K**) Articular cartilage in control and cKO mice visualised with safranin O and fast green staining. Note also hyperplasia of synovial lining in the cKO mouse (arrows). Lines and error bars on all graphs indicate mean ± 95% CI. All images shown are from female mice and scale bars indicate 50 μm. See Suppl. Figure 3A for H&E images of the IFP from male mice and Suppl. Figure 3C-E,H for data in (**G-J**) separated by females and males.

cartilage itself. However, if loss of Seipin from these tissues caused the cartilage damage observed in the *Bscl2* KO females with generalised lipodystrophy, similar effects would have been expected in the *Gdf5-Cre*-driven *Bscl2* cKO model, as these tissues are targeted in this model.[24] It is also possible that there may have been some influence from mouse strain backgrounds in our study, since the *Bscl2* KO mice were on a pure C57Bl/6J background while the *Gdf5-Cre*-driven *Bscl2* cKO mice were on a mixed C57Bl/6J and FVB background. However, the *Bscl2* cKO mice showed increased susceptibility to the cartilage-damaging effects of HFD feeding, despite the potential confounding influence of the mixed strain background, suggesting that this did not have a major impact.

Regardless of the underlying gene mutation, lipodystrophy patients are known to develop joint abnormalities including OA.[49,50] This supports the notion that it is the lipodystrophy and associated metabolic and inflammatory dysfunction that is at the basis of the detrimental effects on cartilage observed in our model. To what extent the cartilage phenotype is due to systemic factors acting directly on the cartilage or secondary to effects on bone is unclear.

Our study reveals the spatiotemporal development and lineage derivation of the IFP, the largest intra-articular adipose depot implicated in OA. A very recent study reported that the IFP develops from *Col2*-expressing cells.[51] Our findings are consistent with this, and more narrowly define its origin from the *Gdf5*-expressing cells of the embryonic joint interzone. Interestingly, while a fibrous-like IFP template was established during late embryogenesis, lipid-laden adipocytes arose from *Gdf5*-lineage *Pdgfrα*-expressing progenitors within the template only shortly after birth in a seemingly stochastic way, as opposed to the more systematic parallel stacking of clonal cells along the longitudinal axis in the adjacent synovium, as we previously reported.[52] Adipocytes are mechanosensitive, and previous work showed that static mechanical loading in pre-adipocytes can accelerate adipogenic differentiation and stimulate lipid production in vitro.[53] It is therefore possible that mechanical loading of the knee following birth stimulates intra-articular adipocyte development.

Adipocytes in the IFP remained of *Gdf5*-lineage derivation until at least 12 months of age. Postnatal *Cre*-mediated recombination in our lineage-tracing model is unlikely, since the *Gdf5* regulatory sequence used to control *Cre* expression in the *Gdf5-Cre* mouse is insufficient to drive expression in adult healthy or diseased knees.[54,55] Moreover, although *Gdf5* can be expressed during adipogenesis,[56] absent Tom expression in sWAT adipocytes indicates that *Cre* was not expressed during adipose tissue development in our model. Heterogeneity in adipocyte lineage between the intra-articular adipose tissue of different synovial joints was observed, with proximal joints showing fewer adipocytes derived from the embryonic joint interzone. This may be due to the timing and extent of *Gdf5* expression in the different joints during embryonic development. Correspondingly, mice with the *brachypodism* mutation at the locus that encodes *Gdf5* show more severe joint defects at the distal joints such as the knee, forefeet, and hindfeet, than in proximal joints.[57]

Adipocyte lineages can exhibit plasticity; for example, ablation of insulin receptor β using *Myf5-Cre* resulted in adipocytes normally of *Myf5*-lineage developing from other compensatory lineages.[58] In the intra-articular lipodystrophy model, caused by loss of *Bscl2* selectively in *Gdf5*-lineage cells, the residual adipocytes in the IFP remained of *Gdf5* lineage without compensation from other cell lineages. This suggests that the IFP lacks non-*Gdf5*-lineage precursors able to undergo adipogenesis. Indeed, we barely detected *Pdgfrα*-expressing cells in the IFP that were not of *Gdf5* lineage. While the subset(s) of *Pdgfrα*-expressing progenitors that give rise to new adipocytes in the IFP during different life stages and in different contexts remains to be clarified, they include Dpp4+ cells,[51] which we have found to be present within the adult *Gdf5*-lineage population in the mouse knee.[52] The presence of residual adipocytes in the IFP in both generalised and selective intra-articular lipodystrophic mice suggests that these cells do not absolutely require Seipin, encoded by *Bscl2*, for their development or maintenance.

In summary, our study reveals the spatiotemporal development and lineage derivation of the IFP, the largest intra-articular adipose depot implicated in OA. We show that while generalised lipodystrophy affects cartilage health in female mice, selective disruption of intra-articular adipose tissue does not drive pathogenic changes to cartilage at homeostasis, with age, or after injury. However,

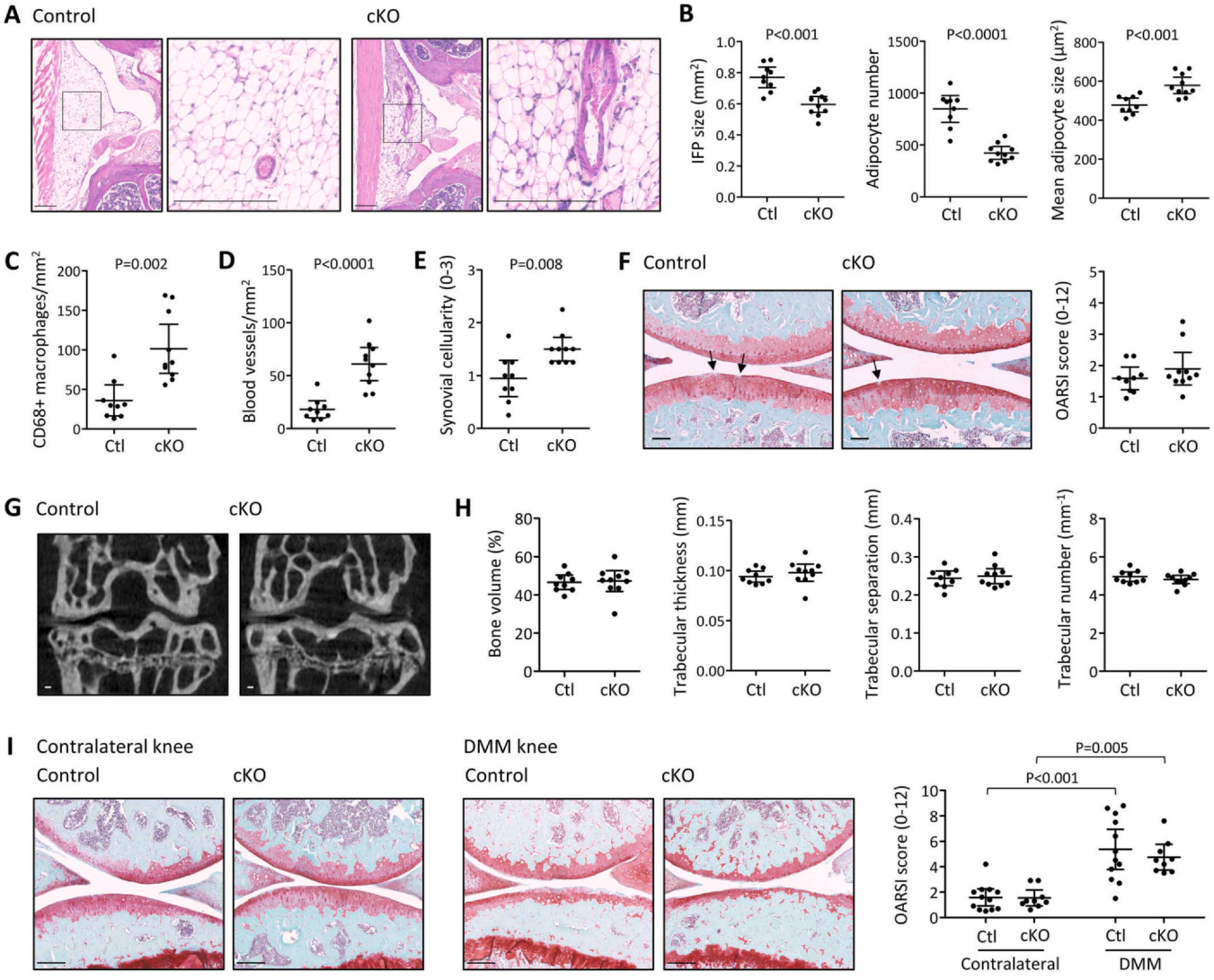

Fig. 4

Osteoarthritis and Cartilage

Effect of intra-articular lipodystrophy on the knee with age and after surgical induction of OA. (**A-H**) Shown are pooled data from 2 cohorts of 10 *Bscl2* cKO and 9 genotype control (Ctl) female mice analysed at 12 months of age. (**A**) Typical morphology of the IFP, visualised by H&E staining. (**B**) IFP size, adipocyte number, and mean adipocyte size, quantified from H&E-stained sections. P-values: unpaired two-tailed Student's t-test. (**C**) Macrophages within the IFP quantified from CD68 immunohistochemically stained sections. P-value: Mann-Whitney U test. (**D**) Blood vessel number quantified from H&E-stained sections. P-value: unpaired two-tailed Student's t-test. (**E**) Cellularity of the synovium surrounding the IFP scored from H&E-stained sections. P-value: Mann-Whitney U test. (**F**) Articular cartilage damage, quantified from safranin O and fast green-stained sections. Arrows indicate cartilage lesions. OARSI scores are shown as the average of the highest 5 summed tibia and femur scores. (**G**) MicroCT images showing bone structure of distal femur (top) and proximal tibia (bottom). (**H**) Tibial subchondral bone parameters quantified by µCT analysis. (**I**) Articular cartilage damage in 12 genotype control (Ctl) and 9 *Bscl2* cKO male mice 6 weeks after surgical destabilisation of the medial meniscus (DMM) at 3 months of age, quantified from safranin O and fast green-stained sections. Shown are pooled data from 3 experiments with similar numbers of genotype control and Bscl2 cKO mice in each experiment. OARSI scores are shown as the average of the highest 5 summed tibia and femur scores. P-values: Kruskal-Wallis test with Dunn's post-test. Lines and error bars on all graphs indicate mean ± 95% CI. Scale bars on all images indicate 100 µm.

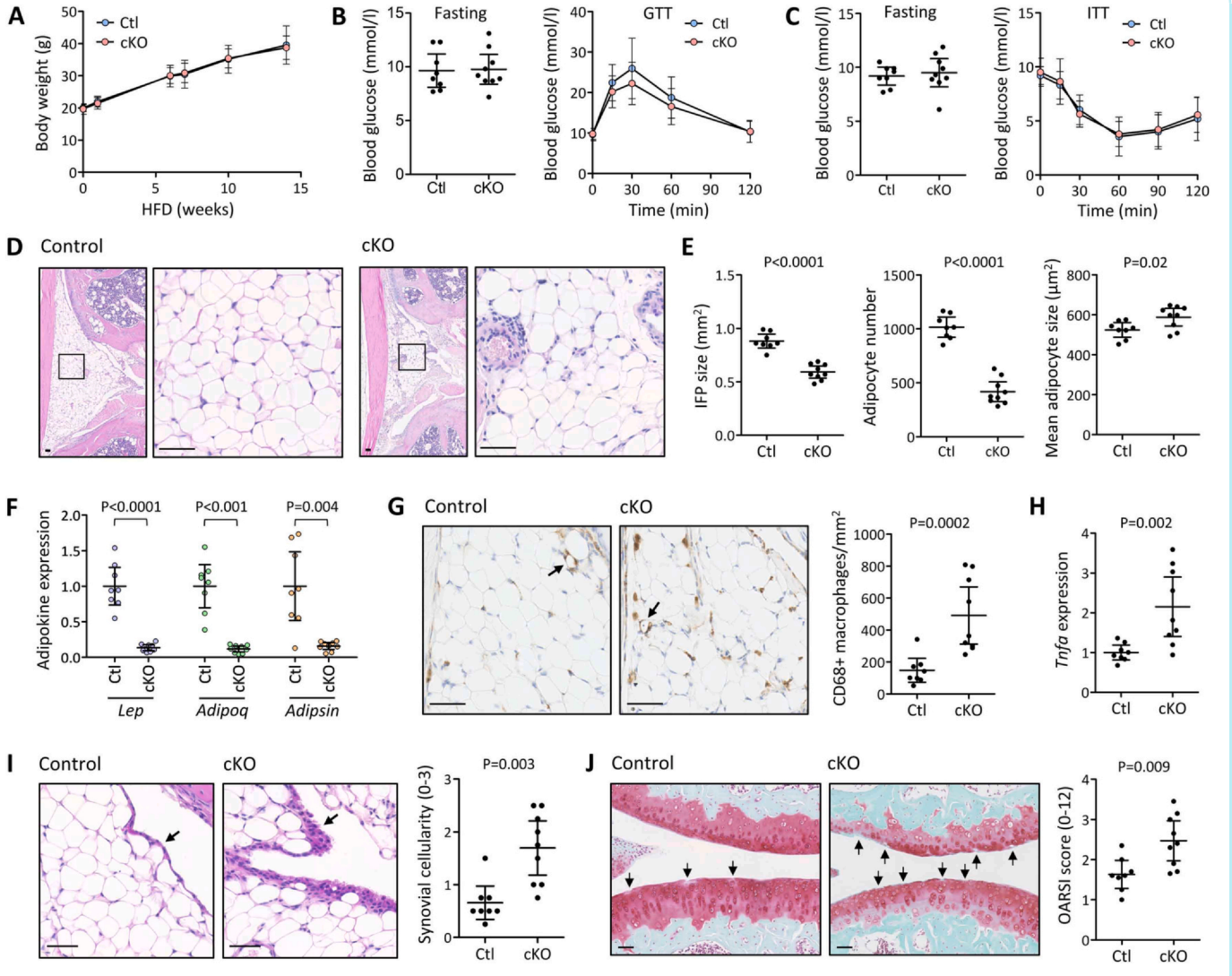

Fig. 5

Osteoarthritis and Cartilage

Effect of HFD-induced obesity in mice with intra-articular lipodystrophy. Shown are data from 9 *Bscl2* cKO and 8 genotype control (Ctl) female mice following HFD feeding from 2 months of age for 14–15 weeks, pooled from 3 experiments with similar numbers of genotype control and *Bscl2* cKO mice in each experiment. (**A**) Body weights during the HFD feeding period. (**B,C**) Fasting blood glucose and GTT (**C**) or ITT (**D**) performed after 10 and 11 weeks of HFD feeding, respectively. (**D**) Typical morphology of the IFP, visualised by H&E staining. (**E**) IFP size, adipocyte number, and mean adipocyte size, quantified from H&E-stained sections. P-values: unpaired two-tailed Student's t-test. (**F**) Expression of the adipokines *Lep*, *Adipoq* and *Adipsin* in the IFP, quantified by RT-qPCR and shown relative to the average in the control group. P-values: unpaired two-tailed Student's t-test after log transformation (*Lep*), Mann-Whitney U test (*Adipoq*), and unpaired two-tailed Welch's t-test (*Adipsin*). (**G**) Macrophages within the IFP, detected by CD68 IHC (brown) with haematoxylin counterstain (blue). P-value: unpaired two-tailed Student's t-test after log transformation. Note the presence of crown-like structures typical of obesity (arrows). (**H**) Expression of *Tnfa* in the IFP, quantified by RT-qPCR and shown relative to the average in the control group. P-value: unpaired two-tailed Student's t-test after log transformation. (**I**) Cellularity of the synovium surrounding the IFP (arrows), scored from H&E-stained sections. P-value: Mann-Whitney U test. (**J**) Articular cartilage damage, quantified from safranin O and fast green-stained sections. Arrows indicate cartilage lesions. OARSI scores are shown as the average of the highest 5 summed tibia and femur scores. P-values: Mann-Whitney U test. Lines and error bars on all graphs represent mean ± 95% CI. Scale bars on all images indicate 50 µm.

disruption of this adipose depot predisposes to the cartilage-damaging effects of HFD-induced obesity. These findings reveal that intra-articular adipose tissue, whilst dispensable for normal joint development and maintenance, can influence how the joint responds to systemic drivers of cartilage damage.

Ethical approval

Animal experimental protocols were approved by the UK Home Office and the Animal Welfare and Ethical Review Committee of the University of Aberdeen.

Funding

This work was supported by funding from Versus Arthritis (grants 20775 and 21156), the Medical Research Council (grant MR/L002620/1), Diabetes UK (grant 18/0005884), the Wellcome Trust through an Institutional Strategic Support Fund, and the NHS Grampian Research Endowment Trust (grant 16/11/032). The study sponsors had no involvement in study design; collection, analysis, and interpretation of data; writing of the manuscript; or the decision to submit the manuscript for publication.

Author contributions

J.J.M.: Experimental design, data acquisition, analysis and interpretation, writing of the manuscript. G.D.M.: Experimental design, data acquisition, analysis and interpretation. R.A.S.: Data acquisition and analysis, contributed to writing of the manuscript. S.M.C., I.C., K.K.: Data acquisition and analysis. W.H.: Provision of resources. F.C.: Data analysis. J.J.R.: Conceptualisation, experimental design, data interpretation. C.D.B.: Conceptualisation, experimental design, data interpretation, writing of the manuscript. A.J.R.: Conceptualisation, experimental design, data acquisition, analysis and interpretation, writing of the manuscript. All authors edited and approved the manuscript.

Conflict of interest

C.D.B. and A.J.R. have received research grant funding through the institution from Biosplice Therapeutics (formerly Samumed LLC). C.D.B. has received consultancy fees or honoraria from UCB, Galapagos and Celltrion Healthcare.

Data Availability

All data supporting the findings of this study are available within the Article and its Supplementary Information files, or are available from the corresponding author upon reasonable request.

Acknowledgements

The authors thank all members and research project students of the Arthritis and Regenerative Medicine Laboratory at the University of Aberdeen. The authors are also grateful to Animal Facility staff for care of our animals, and staff in the Microscopy and Histology Facility and the qPCR Facility for their expert support. Part of this work has been previously presented at OARSI 2022 World Congress: J.J. McClure, G.D. McIlroy., F. Colella, R.A. Symons, S.M. Clark, J.J. Rochford, C. De Bari, A.J. Roelofs. Decreased intra-articular adipose tissue in the knee joint does not affect osteoarthritis development in mice. Osteoarthr Cartil 2022;30:S334.

Appendix A. Supporting information

Supplementary data associated with this article can be found in the online version at doi:10.1016/j.joca.2024.07.006.

References

1. Zheng H, Chen C. Body mass index and risk of knee osteoarthritis: systematic review and meta-analysis of prospective studies. BMJ Open 2015;5(12), e007568. https://doi.org/10.1136/BMJOPEN-2014-007568
2. Henninger AMJ, Eliasson B, Jenndahl LE, Hammarstedt A. Adipocyte hypertrophy, inflammation and fibrosis characterize subcutaneous adipose tissue of healthy, non-obese subjects predisposed to type 2 diabetes. 2014;9, e105262. https://doi.org/10.1371/journal.pone.0105262
3. Berry R, Rodeheffer MS. Characterization of the adipocyte cellular lineage in vivo. Nat Cell Biol 2013;15(3):302–8. https://doi.org/10.1038/ncb2696
4. Wang QA, Tao C, Gupta RK, Scherer PE. Tracking adipogenesis during white adipose tissue development, expansion and regeneration. Nat Med 2013;19(10):1338–44. https://doi.org/10.1038/nm.3324
5. Klein-Wieringa IR, Kloppenburg M, Bastiaansen-Jenniskens YM, Yusuf E, Kwekkeboom JC, El-Bannoudi H, *et al*. The infrapatellar fat pad of patients with osteoarthritis has an inflammatory phenotype. Ann Rheum Dis 2011;70(5):851–7. https://doi.org/10.1136/ard.2010.140046
6. Urban H, Little CB. The role of fat and inflammation in the pathogenesis and management of osteoarthritis. Rheumatology 2018;57(suppl_4):iv10–21. https://doi.org/10.1093/rheumatology/kex399
7. Favero M, El-Hadi H, Belluzzi E, Granzotto M, Porzionato A, Sarasin G, *et al*. Infrapatellar fat pad features in osteoarthritis: a histopathological and molecular study. Rheumatology 2017;56(10):1784–93. https://doi.org/10.1093/rheumatology/kex287
8. Rochford JJ. When adipose tissue lets you down: understanding the functions of genes disrupted in lipodystrophy. Diabetes 2022;71(4):589–98. https://doi.org/10.2337/dbi21-0006
9. Patni N, Garg A. Congenital generalized lipodystrophies—new insights into metabolic dysfunction. Nat Rev Endocrinol 2015;11(9):522–34. https://doi.org/10.1038/nrendo.2015.123
10. Mcilroy GD, Suchacki K, Roelofs AJ, Yang W, Fu Y, Bai B, *et al*. Adipose specific disruption of seipin causes early-onset generalised lipodystrophy and altered fuel utilisation without severe metabolic disease. Mol Metab 2018;10:55–65. https://doi.org/10.1016/j.molmet.2018.01.019
11. Fischer-Posovszky P, Wang QA, Asterholm IW, Rutkowski JM, Scherer PE. Targeted deletion of adipocytes by apoptosis leads to adipose tissue recruitment of alternatively activated M2 macrophages. Endocrinology 2011;152(8):3074–81. https://doi.org/10.1210/en.2011-1031
12. Liu L, Jiang Q, Wang X, Zhang Y, Lin RCY, Lam SM, *et al*. Adipose-specific knockout of seipin/Bscl2 results in progressive lipodystrophy. Diabetes 2014;63(7):2320–31. https://doi.org/10.2337/db13-0729
13. Payne VA, Grimsey N, Tuthill A, Virtue S, Gray SL, Dalla Nora E, *et al*. The Human lipodystrophy gene BSCL2/SEipin May Be Essential for Normal Adipocyte Differentiation. Diabetes 2008;57(8):2055–60. https://doi.org/10.2337/db08-0184
14. Salo VT, Li S, Vihinen H, Hölttä-Vuori M, Szkalisity A, Horvath P, *et al*. Seipin facilitates triglyceride flow to lipid droplet and counteracts droplet ripening via endoplasmic reticulum contact. Dev Cell 2019;50(4):478–493.e9. https://doi.org/10.1016/J.DEVCEL.2019.05.016

15. Sim MFM, Persiani E, Talukder MMU, Mcilroy GD, Roumane A, Edwardson JM, *et al*. Oligomers of the lipodystrophy protein seipin may co-ordinate GPAT3 and AGPAT2 enzymes to facilitate adipocyte differentiation. Sci Rep 2020;10(1):3259. https://doi.org/10.1038/s41598-020-59982-5
16. Cui X, Wang Y, Tang Y, Liu Y, Zhao L, Deng J, *et al*. Seipin ablation in mice results in severe generalized lipodystrophy. Hum Mol Genet 2011;20(15):3022–30. https://doi.org/10.1093/hmg/ddr205
17. Altay C, Secil M, Demir T, Atik T, Akinci G, Ozdemir Kutbay N, *et al*. Determining residual adipose tissue characteristics with MRI in patients with various subtypes of lipodystrophy. Diagnostic Interv Radiol 2017;23(6):428–34. https://doi.org/10.5152/dir.2017.17019
18. Simha V, Agarwal AK, Aronin PA, Iannaccone ST, Garg A. Novel subtype of congenital generalized lipodystrophy associated with muscular weakness and cervical spine instability. Am J Med Genet Part A 2008;146A(18):2318–26. https://doi.org/10.1002/AJMG.A.32457
19. Rountree RB, Schoor M, Chen H, Marks ME, Harley V, Mishina Y, *et al*. BMP Receptor Signaling Is Required for Postnatal Maintenance of Articular Cartilage. PLoS Biol 2004;2(11), e355. https://doi.org/10.1371/journal.pbio.0020355
20. Madisen L, Zwingman TA, Sunkin SM, Oh SW, Zariwala HA, Gu H, *et al*. A robust and high-throughput Cre reporting and characterization system for the whole mouse brain. Nat Neurosci 2010;13(1):133–40. https://doi.org/10.1038/nn.2467
21. Snippert HJ, van der Flier LG, Sato T, van Es JH, van den Born M, Kroon-Veenboer C, *et al*. Intestinal crypt homeostasis results from neutral competition between symmetrically dividing Lgr5 stem cells. Cell 2010;143(1):134–44. https://doi.org/10.1016/j.cell.2010.09.016
22. Hamilton TG, Klinghoffer RA, Corrin PD, Soriano P. Evolutionary divergence of platelet-derived growth factor alpha receptor signaling mechanisms. Mol Cell Biol 2003;23(11):4013. https://doi.org/10.1128/MCB.23.11.4013-4025.2003
23. Roumane A, Mcilroy GD, Balci A, Han W, Delibegović M, Baldassarre M, *et al*. Bscl2 deficiency does not directly impair the innate immune response in a murine model of generalized lipodystrophy. J Clin Med 2021;10(3):441. https://doi.org/10.3390/jcm10030441
24. Roelofs AJ, Zupan J, Riemen AHK, Kania K, Ansboro S, White N, *et al*. Joint morphogenetic cells in the adult mammalian synovium. Nat Commun 2017;8(1), 15040. https://doi.org/10.1038/ncomms15040
25. Glasson SS, Blanchet TJ, Morris EA. The surgical destabilization of the medial meniscus (DMM) model of osteoarthritis in the 129/SvEv mouse. Osteoarthritis Cartilage 2007;15(9):1061–9. https://doi.org/10.1016/j.joca.2007.03.006
26. Ma HL, Blanchet TJ, Peluso D, Hopkins B, Morris EA, Glasson SS. Osteoarthritis severity is sex dependent in a surgical mouse model. Osteoarthritis Cartilage 2007;15(6):695–700. https://doi.org/10.1016/J.JOCA.2006.11.005
27. Symons RA, Colella F, Collins FL, Rafipay AJ, Kania K, McClure JJ, *et al*. Targeting the IL-6–Yap–Snail signalling axis in synovial fibroblasts ameliorates inflammatory arthritis. Ann Rheum Dis 2022;81(2):214–24. https://doi.org/10.1136/annrheumdis-2021-220875
28. Roelofs AJ, De Bari C. Immunostaining of Skeletal Tissues. Humana Press Inc.; 2019. p. 437–50. https://doi.org/10.1007/978-1-4939-8997-3_25
29. Bankhead P, Loughrey MB, Fernández JA, Dombrowski Y, McArt DG, Dunne PD, *et al*. QuPath: Open source software for digital pathology image analysis. Sci Rep 2017;7(1), 16878. https://doi.org/10.1038/s41598-017-17204-5
30. Osman OS, Selway JL, Kępczyńska MA, Stocker CJ, O'Dowd JF, Cawthorne MA, *et al*. A novel automated image analysis method for accurate adipocyte quantification. Adipocyte 2013;2(3):160–4. https://doi.org/10.4161/adip.24652
31. Glasson SS, Chambers MG, Van Den Berg WB, Little CB. The OARSI histopathology initiative – recommendations for histological assessments of osteoarthritis in the mouse. Osteoarthritis Cartilage 2010;18:S17–23. https://doi.org/10.1016/j.joca.2010.05.025
32. Jackson MT, Moradi B, Zaki S, Smith MM, McCracken S, Smith SM, *et al*. Depletion of protease-activated receptor 2 but not protease-activated receptor 1 may confer protection against osteoarthritis in mice through extracartilaginous mechanisms. Arthritis Rheumatol 2014;66(12):3337–48. https://doi.org/10.1002/art.38876
33. Van Maldergem L. Genotype-phenotype relationships in Berardinelli-Seip congenital lipodystrophy. J Med Genet 2002;39(10):722–33. https://doi.org/10.1136/jmg.39.10.722
34. Raygada M, Rennert O. Congenital generalized lipodystrophy: profile of the disease and gender differences in two siblings. Clin Genet 2004;67(1):98–101. https://doi.org/10.1111/j.1399-0004.2004.00372.x
35. Shwartz Y, Viukov S, Krief S, Zelzer E. Joint development involves a continuous influx of Gdf5-positive cells. Cell Rep 2016;15(12):2577. https://doi.org/10.1016/J.CELREP.2016.05.055
36. Griffin TM, Huebner JL, Kraus VB, Yan Z, Guilak F. Induction of osteoarthritis and metabolic inflammation by a very high-fat diet in mice: effects of short-term exercise. Arthritis Rheum 2012;64(2):443–53. https://doi.org/10.1002/art.33332
37. Chong TKY, Tan JR, Ma CA, Wong SBS, Leung YY. Association of adipokines with severity of knee osteoarthritis assessed clinically and on magnetic resonance imaging. Osteoarthr Cartil Open 2023;5(4), 100405. https://doi.org/10.1016/J.OCARTO.2023.100405
38. Paré F, Tardif G, Fahmi H, Ouhaddi Y, Pelletier JP, Martel-Pelletier J. In vivo protective effect of adipsin-deficiency on spontaneous knee osteoarthritis in aging mice. Aging 2020;12(3):2880. https://doi.org/10.18632/AGING.102784
39. Zhu H, Zhou L, Wang Q, Cai Q, Yang F, Jin H, *et al*. Glucagon-like peptide-1 receptor agonists as a disease-modifying therapy for knee osteoarthritis mediated by weight loss: findings from the Shanghai Osteoarthritis Cohort. Ann Rheum Dis 2023;82:1218–26. https://doi.org/10.1136/ard-2023-223845
40. Graney PL, Ben-Shaul S, Landau S, Bajpai A, Singh B, Eager J, *et al*. Macrophages of diverse phenotypes drive vascularization of engineered tissues. Sci Adv 2020;6(18), eaay6391. https://doi.org/10.1126/SCIADV.AAY6391/SUPPL_FILE/AAY6391_SM.PDF
41. Onogi Y, Wada T, Okekawa A, Matsuzawa T, Watanabe E, Ikeda K, *et al*. Pro-inflammatory macrophages coupled with glycolysis remodel adipose vasculature by producing platelet-derived growth factor-B in obesity. Sci Rep 2020;10(1):1–13. https://doi.org/10.1038/s41598-019-57368-w
42. Yan J, Horng T. Lipid metabolism in regulation of macrophage functions. Trends Cell Biol 2020;30(12):979–89. https://doi.org/10.1016/J.TCB.2020.09.006
43. Wueest S, Rapold RA, Rytka JM, Schoenle EJ, Konrad D. Basal lipolysis, not the degree of insulin resistance, differentiates large from small isolated adipocytes in high-fat fed mice. Diabetologia 2009;52(3):541–6. https://doi.org/10.1007/s00125-008-1223-5
44. Medina-Luna D, Santamaría-Olmedo MG, Zamudio-Cuevas Y, Martínez-Flores K, Fernández-Torres J, Martínez-Nava GA, *et al*. Hyperlipidemic microenvironment conditionates damage mechanisms in human chondrocytes by oxidative stress. Lipids Health Dis 2017;16(1):1–8⟨https://doi.org/10.1186/S12944-017-0510-X/FIGURES/6⟩.

45. Roumane A, Mcilroy GD, Sommer N, Han W, Heisler LK, Rochford JJ. GLP-1 receptor agonist improves metabolic disease in a pre-clinical model of lipodystrophy. Front Endocrinol 2024;15:1379228. ⟨https://doi.org/10.3389/FENDO.2024.1379228/BIBTEX⟩.
46. Collins KH, Lenz KL, Pollitt EN, Ferguson D, Hutson I, Springer LE, *et al*. Adipose tissue is a critical regulator of osteoarthritis. Proc Natl Acad Sci 2021;118(1), e2021096118. https://doi.org/10.1073/pnas.2021096118
47. Roy B, Palaniyandi SS. Tissue-specific role and associated downstream signaling pathways of adiponectin. Cell Biosci 2021;11(1):77. https://doi.org/10.1186/S13578-021-00587-4
48. Liu F, Dai S, Feng D, Peng X, Qin Z, Kearns AC, *et al*. Versatile cell ablation tools and their applications to study loss of cell functions. Cell Mol Life Sci 2019;76(23):4725–43. https://doi.org/10.1007/s00018-019-03243-w
49. Ajluni N, Meral R, Neidert AH, Brady GF, Buras E, McKenna B, *et al*. Spectrum of disease associated with partial lipodystrophy: lessons from a trial cohort. Clin Endocrinol 2017;86(5):698–707. https://doi.org/10.1111/CEN.13311
50. Teboul-Coré S, Rey-Jouvin C, Miquel A, Vatier C, Capeau J, Robert JJ, *et al*. Bone imaging findings in genetic and acquired lipodystrophic syndromes: an imaging study of 24 cases. Skeletal Radiol 2016;45(11):1495–506⟨https://doi.org/10.1007/S00256-016-2457-9/FIGURES/12⟩.
51. Li J, Gui T, Yao L, Guo H, Lin YL, Lu J, *et al*. Synovium and infrapatellar fat pad share common mesenchymal progenitors and undergo coordinated changes in osteoarthritis. J Bone Miner Res 2024;39(2):161–76. https://doi.org/10.1093/JBMR/ZJAD009
52. Collins FL, Roelofs AJ, Symons RA, Kania K, Campbell E, Collieduguid ESR, *et al*. Taxonomy of fibroblasts and progenitors in the synovial joint at single-cell resolution. Ann Rheum Dis 2023;82(3):428–37. https://doi.org/10.1136/ard-2021-221682
53. Shoham N, Gottlieb R, Sharabani-Yosef O, Zaretsky U, Benayahu D, Gefen A. Static mechanical stretching accelerates lipid production in 3T3-L1 adipocytes by activating the MEK signaling pathway. Am J Physiol Cell Physiol 2012;302(2):429–41. https://doi.org/10.1152/AJPCELL.00167.2011/ASSET/IMAGES/LARGE/ZH00011268270010.JPEG
54. Chen H, Capellini TD, Schoor M, Mortlock DP, Reddi AH, Kingsley DM. Heads, shoulders, elbows, knees, and toes: modular Gdf5 enhancers control different joints in the vertebrate skeleton. PLoS Genet 2016;12(11), e1006454. https://doi.org/10.1371/JOURNAL.PGEN.1006454
55. Kania K, Colella F, Riemen AHK, Wang H, Howard KA, Aigner T, *et al*. Regulation of Gdf5 expression in joint remodelling, repair and osteoarthritis. Sci Rep 2020;10(1):1–11. https://doi.org/10.1038/s41598-019-57011-8
56. Pei Z, Yang Y, Kiess W, Sun C, Luo F. Dynamic profile and adipogenic role of growth differentiation factor 5 (GDF5) in the differentiation of 3T3-L1 preadipocytes. Arch Biochem Biophys 2014;560:27–35. https://doi.org/10.1016/J.ABB.2014.07.025
57. Storm EE, Huynh TV, Copeland NG, Jenkins NA, Kingsley DM, Lee SJ. Limb alterations in brachypodism mice due to mutations in a new member of the TGFβ-superfamily. Nature 1994;368(6472):639–43. https://doi.org/10.1038/368639a0
58. Sanchez-Gurmaches J, Guertin DA. Adipocytes arise from multiple lineages that are heterogeneously and dynamically distributed. Nat Commun 2014;5(1):1–13. https://doi.org/10.1038/ncomms5099